Range accuracy of a Gated-Viewing system as a function of the gate shift step size

Benjamin Göhler*, Peter Lutzmann
Fraunhofer Institute of Optronics, System Technologies and Image Exploitation (IOSB),
Department Optronics, Gutleuthausstrasse 1, 76275 Ettlingen, Germany

ABSTRACT

Primarily, a Gated-Viewing (GV) system provides range gated imagery. By increasing the camera delay time from frame to frame, a so-called sliding gates sequence is obtained by which 3-D reconstruction is possible. An important parameter of a sliding gates sequence is the step size by which the gate is shifted. In order to reduce the total number of required images, this step size should be as large as possible without significantly degrading the range accuracy.

In this paper we have studied the influence of the gate shift step size on the resulting range accuracy. Therefore, we have combined the Intevac Gated-Viewing detector M506 with a pulsed 1.57 µm illumination laser. The maximal laser pulse energy is 65 mJ. The target is a one-square-meter-plate at a distance of 500 m. The plate is laminated with a Spectralon layer having Lambertian reflection behavior with a homogeneous reflectance of 93 %. For the measurements, this plate was orientated diagonally to the line of sight of the sensor in order to provide a depth scenario. We have considered different combinations of the two parameters »gate length« (13.5 m, 23.25 m, 33 m) and »signal-to-noise ratio« (SNR) (2 dB, 3 dB, 5 dB, 6 dB, 7 dB, 8 dB). For each considered set of parameters, a sliding gates sequence of the target was recorded. Per range, 20 frames were collected. The gate shift step size was set to the minimal possible value, 75 cm. By skipping certain ranges, a sliding gates sequence with a larger gate shift step size is obtained. For example, skipping the ranges 2, 3, 5, 6, 8, 9,… (equivalent: taking the ranges 1, 4, 7, …) results in a gate shift step size of 2.25 m. Finally, the range accuracies were derived as a function of the gate shift step size. Additionally, the influence of frame averaging on these functions was studied.

Keywords: Gated-Viewing, Range gating, Active imaging, SWIR, Sliding gates method, Range accuracy, Temporal frame averaging

1. INTRODUCTION

In the past few years, a lot of work has been done concerning the 3-D capability of gated imaging systems. Basically, two approaches can be recognized. The first, intuitive technique is the so-called »sliding gates« method[1-5]. Simply, by increasing continuously the distance between the range gate and the sensor during image capturing, a range sampled sequence of the scenery is obtained. By sticking together images showing consecutive range gates, 3-D reconstruction of the objects in the field of view (FOV) is achieved. The second, sophisticated approach makes use of multiple exposures of range gated images in order to create coded images[6-7]. A direct control access to the sensor gate is required. The 3-D reconstruction is based on the comparison of pixel grey level values in a certain number of coded images.

An important parameter of the former approach is the step size by which the gate is shifted to obtain the sliding gates sequence. The smaller the step size, the higher the range resolution. But then, on the other hand, more gate positions and therefore, more emitted laser pulses are required in order to cover the whole object of interest. From a military point of view, it is not desired to emit a large number of laser pulses because each laser pulse can reveal the own position. Furthermore, a longer recording time could lead to a degradation of range accuracy in dynamic scenarios when the object is moving relatively to the sensor.

Since the sliding gates method is based on the detected laser intensity, it suffers from the scintillation effect induced by atmospheric turbulence. A common technique to mitigate this degrading effect is to reduce the standard deviation of

*benjamin.goehler@iosb.fraunhofer.de; phone +49 7243 992-260; fax +49 7243 992-299; www.iosb.fraunhofer.de

Electro-Optical Remote Sensing, Photonic Technologies, and Applications VII; and Military Applications in Hyperspectral Imaging and High Spatial Resolution Sensing, edited by G. W. Kamerman, O. K. Steinvall, G. J. Bishop, J. D. Gonglewski, Proc. of SPIE Vol. 8897, 889708 · © 2013 SPIE · CCC code: 0277-786X/13/$18 · doi: 10.1117/12.2029590

this intensity fluctuation by averaging, pixel by pixel, several images for each gate position before processing.

Within the framework of this paper, as a continuation of previous work[8], the influence of the gate shift step size (GSSS) on the range accuracy derived from the sliding gates method is investigated. Different combinations of the three parameters »number of averaged images per range«, »gate length« and »SNR« (defined by equation (1)) are considered. In Section 2 the experimental set-up for data collection is illustrated. Section 3 shows data examples. The methodology that was employed for the range accuracy analysis of the data is described in Section 4. The main results of the range error analysis are contained in Section 5. Finally in Section 6, conclusions are drawn.

2. EXPERIMENTAL SET-UP

A flash lamp pumped Nd:YAG Q-switched laser with a maximal pulse energy of 65 mJ, a wavelength of 1.57 µm (OPO shifted) and a pulse width of 7.1 ns is synchronized with the Intevac GV detector LIVAR® M506 with a full resolution of 1280x1024 pixels and a detector pitch of 6.7 µm. The laser is equipped with a beam shaper[9] with a transmission of 70 % producing speckle-reduced illumination with a homogeneous flat top profile. The divergence of the outgoing laser pulse is 1°. With an additional attachment, a divergence of 0.25° is possible. Optics with a focal length of 500 mm and a F-number of 3.3 is mounted in front of the GV detector. Additionally, the Scintec Boundary Layer Scintillometer (BLS) 900 receiver is mounted next to the GV system. At a distance of 500 m the Scintec BLS900 transmitter and a one-square-meter-plate are positioned next to each other. The plate is laminated with a Spectralon layer having Lambertian reflection behavior with a homogeneous reflectance of 93 %. The plate is orientated diagonally to the line of sight of the GV system in order to provide a depth scenario. A scheme of the experimental set-up is depicted in Figure 1.

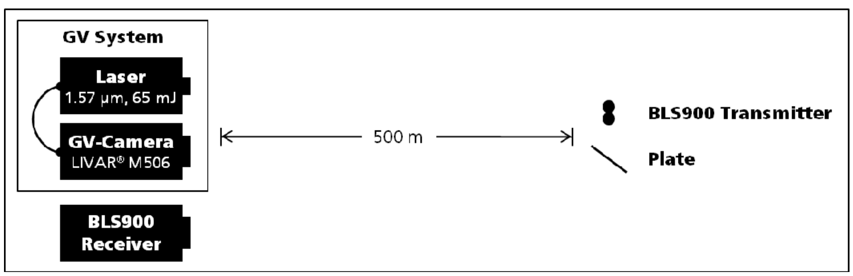

Figure 1. Scheme of the experimental set-up for measurements. Left: GV system (laser and GV camera) and scintillometer receiver. Right: Scintillometer transmitter and target (plate) at a distance of 500 m.

The BLS900 provides measurements of the refractive index structure parameter C_n^2 [$m^{-2/3}$] and the crosswind $v_\perp$ [m/s] during the GV data collection. The GV detector was operated in a 2x2 binning mode, resulting in an image resolution of 640x512 pixels and a virtual pixel size of 13.4 µm. The horizontal FOV is approximately 1°. In this configuration the system is nearly diffraction-limited with an Airy disc diameter of 12.8 µm.

3. DATA

For data collection, the frame rate is set to 10 Hz. The gate is shifted by the minimal possible value of 75 cm corresponding to a time-of-flight of 5 ns (200 MHz clock time). For each range, 20 images are captured for subsequent averaging. Different combinations of the following parameters were considered:

- **Gate length (number of ranges / gate start):** 13.5 m (35/488 m), 23.25 m (50/478.25 m), 33 m (65/464 m)
- **Divergence of the outgoing laser pulse:** 0.25°, 1°
- **Laser energy transmission:** 5 %, 10 %, 25 %, 50 %, 75 %

The »divergence of the outgoing laser pulse« (parameter 2) and the »laser energy transmission« (parameter 3) can be combined into a single value describing the maximal brightness of the target in the sliding gates sequence compared to its noise floor. The resulting value is defined as SNR [dB] by

$$SNR = 10 \cdot \log_{10} \frac{G_{\max}}{G_{\min}}, \qquad (1)$$

where G_{max} and G_{min} denote the maximal and minimal value of the average target grey levels after averaging 20 frames per range. Exemplarily, in Figure 2, the average target grey levels are plotted against the range number in the sliding gates sequence after averaging 20 frames per range. Three curves are depicted for the gate lengths mentioned above.

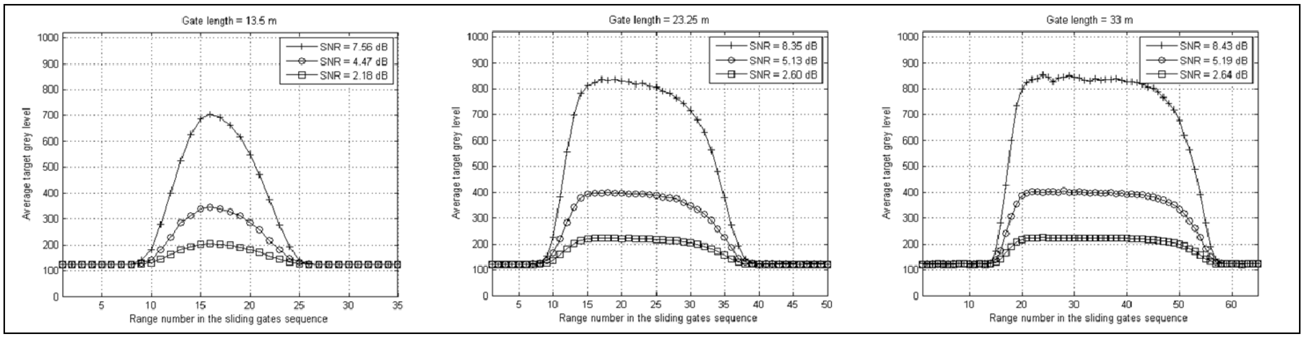

Figure 2. Plots of the average target grey level against the range number in the sliding gates sequence after averaging 20 frames per range. From the maximal and minimal values of these curves, the SNR is derived by Equation (1). The gate lengths are 13.5 m (left), 23.25 m (middle) and 33 m (right). The gate was shifted 35 times (left), 50 times (middle) and 65 times (right) by 75 cm and the divergence of the outgoing laser pulse was 1°. The laser energy transmissions were 75 % (+), 25 % (○) and 10 % (□).

In the upper right corner of the plots in Figure 2, the resulting SNR values are given for the 3 exemplary curves. These SNR values are calculated for all sliding gates sequences and will replace the two parameters »divergence of the outgoing laser pulse« and »laser energy transmission« mentioned above. They are rounded to the closest integer and take the following values.

- **SNR:** 2 dB, 3 dB, 5 dB, 6 dB, 7 dB, 8 dB

Exemplarily, Figure 3 shows a part of a sliding gates sequence. The first 10 and the last 7 ranges are skipped. Each GV image in this sequence is cropped to the target and enlarged. The gate length is 13.5 m and the SNR is 8 dB.

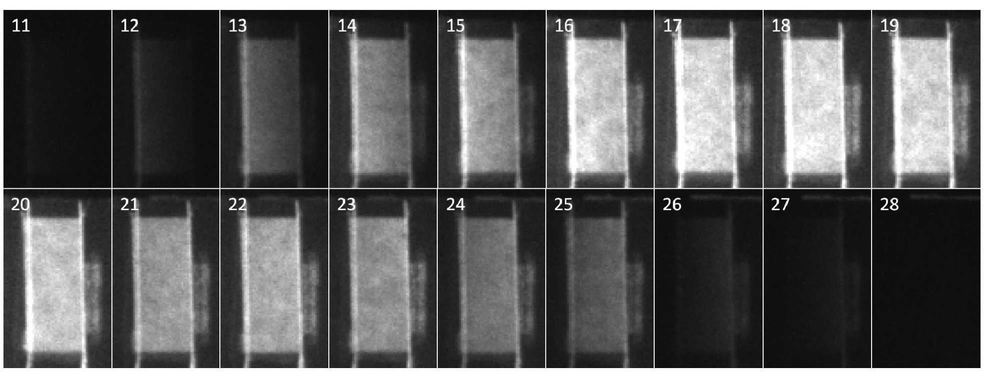

Figure 3. Part of a sliding gates sequence with a gate length of 13.5 m and a SNR of 8 dB.

		Gate length		
		13.5 m	23.25 m	33 m
SNR	1 dB			
	2 dB	✓		
	3 dB		✓	✓
	4 dB			
	5 dB	✓	✓	✓
	6 dB	✓		
	7 dB	✓	✓	✓
	8 dB		✓	✓
	9 dB			

Figure 4. Overview of the 12 data sets (✓) for further analysis. The arrows indicate associated data (same laser beam divergence and same laser energy transmission).

The table in Figure 4 gives an overview of the 12 data sets that will be studied in the following. For each gate length, there are 4 series of measurements with different SNR values: 2/3 dB, 5 dB, 6/7 dB and 7/8 dB. The reason for the decreased SNR values for a gate length of 13.5 m (compared to 23.25 m and 33 m) is a too short gate. The average target grey level in the left graph of Figure 2 does not reach the plateaus of the curves in the middle and right plots although the divergence of the outgoing laser pulse (1°) and the laser energy transmission (75 % (+), 25 % (○) and 10 % (□)) are the same. That is because the high-voltage (HV) between the photocathode and the CMOS sensor is switched off before reaching its maximum. The time that is required for the HV rising and falling slope is 65 ns each. Thus, the minimal integration time without clipping like above is 130 ns corresponding to a gate length of 19.5 m.

During the GV data collection, the BLS900 provided C_n^2 values between $0.2\cdot10^{-14}$ $m^{-2/3}$ and $3\cdot10^{-14}$ $m^{-2/3}$ and crosswind values between 3 m/s and 12 m/s. The Greenwood time constant τ_G is the time interval over which turbulence stays constant. Under the assumption of constant C_n^2 and crosswind values along the propagation path of the laser pulse, τ_G can be estimated by[10]

$$\tau_G = \frac{(2.91\cdot k^2\cdot C_n^2\cdot L)^{-3/5}}{v_\perp}, \tag{2}$$

where $k = 2\pi/\lambda$ [m^{-1}] is the wavenumber, λ [m] is the laser wavelength and L [m] is the length of the laser pulse propagation path. For a wavelength of $\lambda = 1.57$ µm, a path length of L = 500 m and the weakest turbulence and crosswind conditions of $0.2\cdot10^{-14}$ $m^{-2/3}$ and 3 m/s, respectively, during the GV data collection, the Greenwood time constant is calculated with Equation (2) to τ_G = 33 ms. Thus, a frame rate of 10 Hz is sufficiently small to capture images with pairwise uncorrelated intensity disturbances due to scintillation. So, they are suited for frame averaging.

4. METHODOLOGY

The 12 considered sliding gates sequences shown in Figure 4 are processed with the same algorithm to derive a range value for each pixel. First of all, a region of interest (ROI) within the target area is defined. The size of the ROI is 10x30 pixels for all data sets. By plotting the intensity values of a ROI pixel against the range number in the sliding gates sequence, the intensity profile is obtained that is the convolution of the sensor gate and the laser pulse. This intensity profile is approximated by the symmetric, piecewise polynomial function Π_p in Figure 5 with $p = (p_1,p_2,p_3,p_4,p_5)$, $p_1 \le p_2 \le p_3$, $p_4 \le p_5$.

$$\Pi_p(x) = \begin{cases} p_4 & \text{if} \quad x < p_1 \text{ or } x > p_3 + p_2 - p_1 \\ p_5 & \text{if} \quad p_2 < x < p_3 \\ (p_5 - p_4)\cdot\left[-2\cdot\left(\frac{x-p_1}{p_2-p_1}\right)^3 + 3\cdot\left(\frac{x-p_1}{p_2-p_1}\right)^2\right] + p_4 & \text{if} \quad p_1 \le x \le p_2 \\ (p_5 - p_4)\cdot\left[2\cdot\left(\frac{x-p_3}{p_2-p_1}\right)^3 - 3\cdot\left(\frac{x-p_3}{p_2-p_1}\right)^2\right] + p_5 & \text{if} \quad p_3 \le x \le p_3 + p_2 - p_1 \end{cases}$$

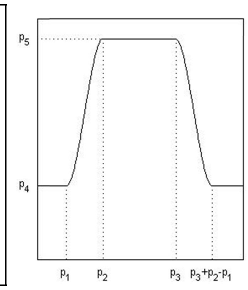

Figure 5. Equation (left) and plot (right) of parameterized symmetric function Π_p with the parameters $p_1,\ldots,p_5$ as approximation of the intensity profile.

In the **first** step, this function is fitted to the measured intensity values for each pixel by the least squares method:

$$\min_p \sqrt{\sum_{k=1}^{n} (\Pi_p(k) - g_k)^2}, \tag{3}$$

where g_k are the pixel grey levels ($k \in \{1,2,\ldots,n\}$) and n is the number of different ranges in the sliding gates sequence.

Exemplarily, some results of these curve fits are shown in Figures 6 to 9 (solid lines) for the 3 gate lengths 13.5 m, 23.25 m and 33 m and for different SNR values. For Figure 6, all ranges in the sliding gates sequence are considered for curve fitting. So here, the gate shift step size (GSSS) is equal to the minimal possible value: GSSS = 0.75 m.

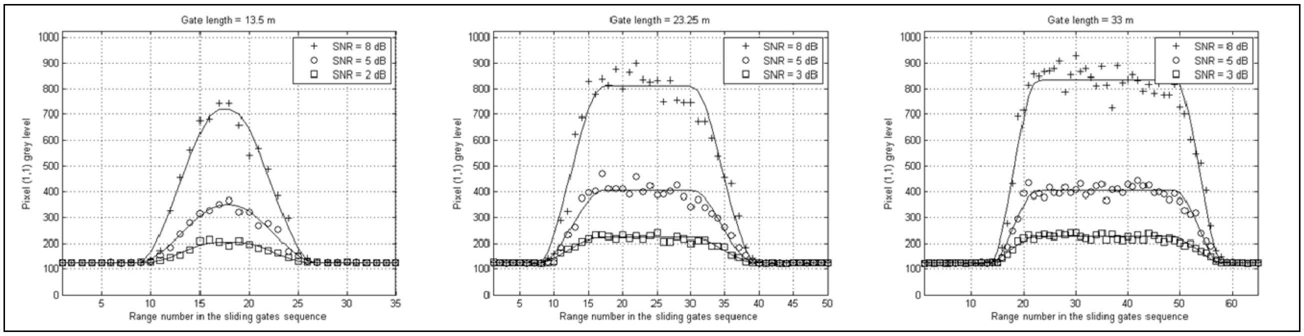

Figure 6. Plots of the grey levels (markers) for ROI pixel (1,1) against the range number in the sliding gates sequence for **GSSS = 0.75 m**. The solid lines are the fitted intensity curves Π_p. The gate lengths are 13.5 m (left), 23.25 m (middle) and 33 m (right) and the SNR values are 8 dB (+), 5 dB (○) and 2/3 dB (□).

It can be seen that the curve fitting step works quite well. But it also turns out that the simple approach from Figure 5 for the intensity profile is not an optimal choice. Especially the middle and right graph show a rounded edge at the transition from the plateau to the falling slope. This rounded edge is not modeled with Π_p. However, the other parts of the intensity profile can be modeled quite well by Π_p. So, this approach will be kept in the following.

For Figures 7, 8 and 9, not all ranges in the sliding gates sequence are considered for curve fitting. By considering each second range (skipping the ranges 1, 3, 5, …), the density of the data points is reduced by a factor of 2 and the graphs in Figure 7 are obtained for GSSS = 1.5 m.

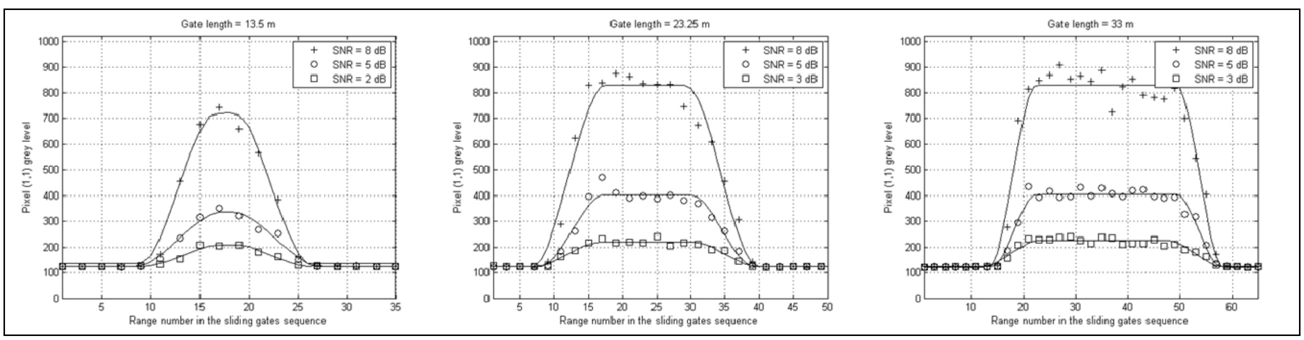

Figure 7. The same as in Figure 6 but for **GSSS = 1.5 m**.

By considering each fourth range 1, 5, 9, … (skipping the ranges 2-4, 6-8, …), the density of the data points is reduced by a factor of 4 and the graphs in Figure 8 are obtained for GSSS = 3 m.

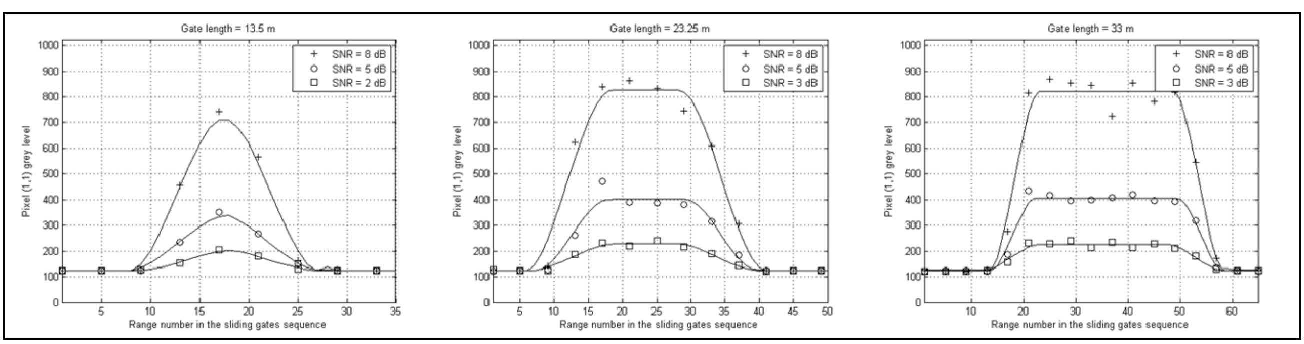

Figure 8. The same as in Figure 6 but for **GSSS = 3 m**.

By considering each seventh range 1, 8, 15, … (skipping the ranges 2-7, 9-14, …), the density of the data points is reduced by a factor of 7 and the graphs in Figure 9 are obtained for GSSS = 5.25 m.

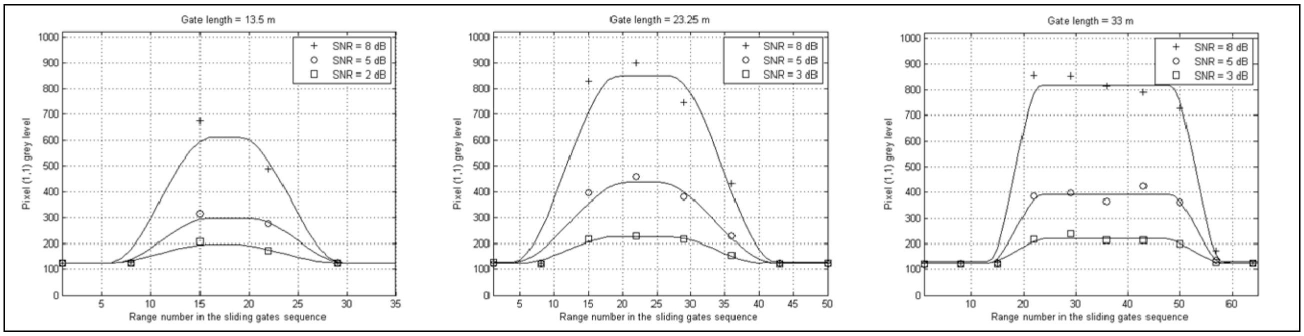

Figure 9. The same as in Figure 6 but for **GSSS = 5.25 m**.

In all graphs of Figures 6 to 9, the step of curve fitting was performed successfully although the density of data points was significantly reduced. However, in the left graph (13.5 m gate length) of Figure 9, a correct reconstruction of the intensity curve (without plateau) was not possible. So here, a degradation of the resulting range accuracy is already expectable.

From the optimal parameters p_2 and p_3, the range is derived by calculating their mean value and converting this real-valued number into the corresponding range by:

$$R = gatestart + \left(\frac{p_2 + p_3}{2} - 1\right) \cdot GSSS + \frac{gatelength}{2} \, . \tag{4}$$

In the **second** step, the range accuracy (or range error) is derived. Therefore, a plane is fitted to the resulting point cloud of the ROI. Let R(x,y) be the calculated range map. (x,y) denotes the horizontal and vertical pixel number in the ROI. The approach for the plane is P(x,y) = ax + by + c, where the parameters a, b and c are again determined by the least squares method:

$$\min_{a,b,c} \sqrt{\sum_{x=1}^{10} \sum_{y=1}^{30} (P(x,y) - R(x,y))^2} \, . \tag{5}$$

Finally, the standard deviation of the difference array D(x,y) = P(x,y) – R(x,y) is defined as range error σ_R:

$$\boxed{\sigma_R = \sqrt{\frac{1}{300} \cdot \sum_{x=1}^{10} \sum_{y=1}^{30} (D(x,y) - \mu_D)^2}} \, , \tag{6}$$

where μ_D is the mean value of D:

$$\mu_D = \frac{1}{300} \cdot \sum_{x=1}^{10} \sum_{y=1}^{30} D(x,y) \, . \tag{7}$$

A small value of μ_D indicates a good fit of P to R. The minimizations in Equations (3) and (5) were realized with the MATLAB® function *fminsearch* that uses a derivative-free simplex search method. The entire procedure for deriving the range error from a sliding gates sequence was carried out for the 12 data sets shown in Figure 4 and, additionally, for 1, 4 and 7 averaged frames per range in order to study also the influence of frame averaging on the obtained range errors.

5. RESULTS

In Figure 10, the range errors are plotted as functions of the gate shift step size. Each range error value is calculated with the procedure described in Section 4. Shown are the results for the gate lengths 13.5 m (left graph), 23.25 m (middle graph) and 33 m (right graph) and for the SNR values 2/3 dB, 5 dB, 6/7 dB and 7/8 dB.

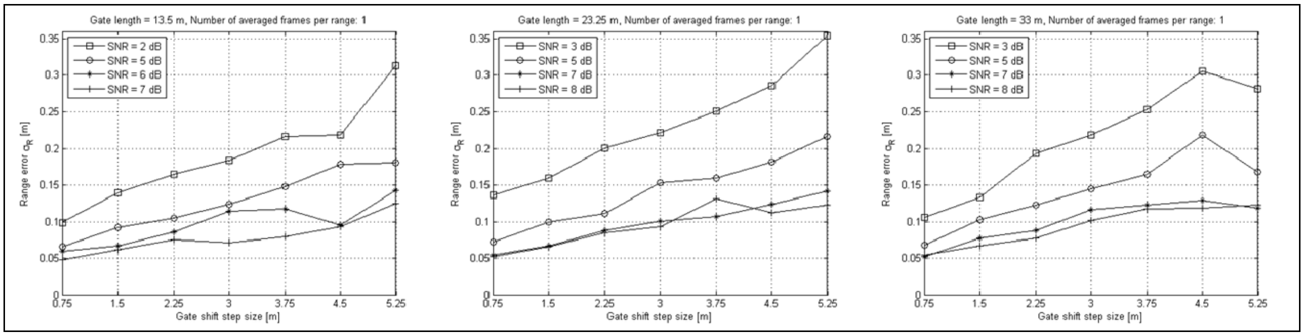

Figure 10. Plots of the range errors σ_R as functions of the gate shift step size for the gate lengths 13.5 m (left graph), 23.25 m (middle graph) and 33 m (right graph). Each graph shows the range error functions for the SNR values 2/3 dB, 5 dB, 6/7 dB and 7/8 dB.

As expected, the curves in Figure 10 roughly show an increasing behavior which means that the range error is degraded with an increased gate shift step size. Approximately, they follow linear laws. The higher the SNR, the lower the range error. There is almost no difference between corresponding curves in the three graphs, so the gate length has no influence on the range error. Roughly, the range error is degraded from 5-14 cm for GSSS = 0.75 m to 12-35 cm for GSSS = 5.25 m (depending on SNR). The range error for GSSS = 0.75 m nearly coincide with previous results[8].

In the following, some results are shown concerning frame averaging for reduction of turbulence induced scintillation. In Figures 11 and 12, the results after averaging 4 and 7 frames per range are depicted, respectively.

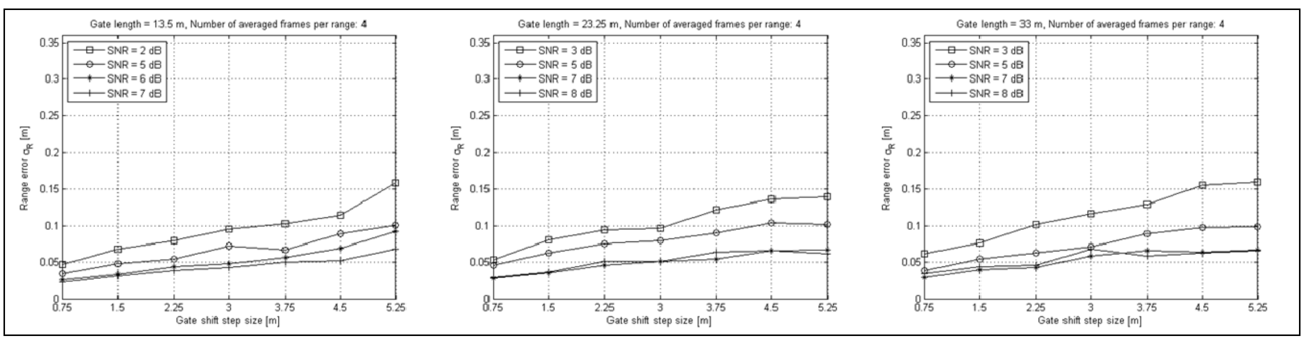

Figure 11. The same as in Figure 10 but after **averaging 4 frames** per range.

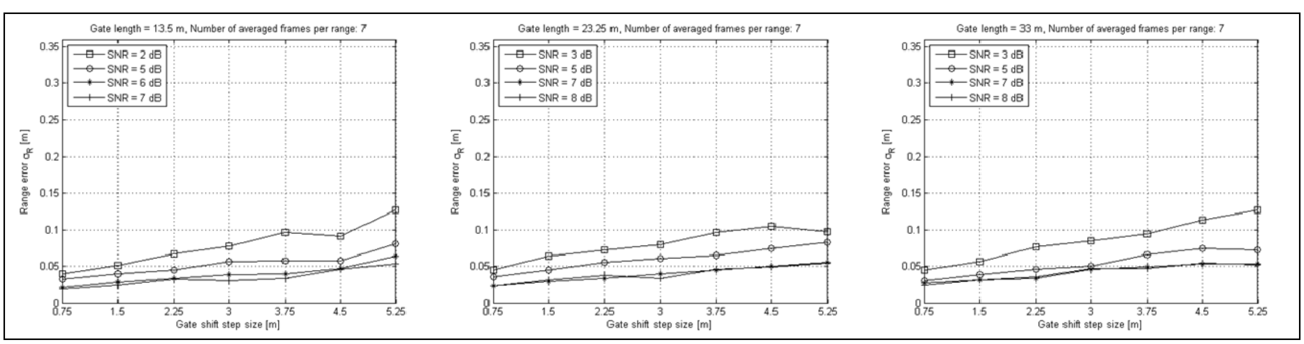

Figure 12. The same as in Figure 10 but after **averaging 7 frames** per range.

Compared to Figure 10, Figure 11 and 12 show significant improvements of the range error. After averaging 4 frames per range (Figure 11), the range error is degraded from 3-5 cm for GSSS = 0.75 m to 7-16 cm for GSSS = 5.25 m (depending on SNR) which means an improvement compared the no averaging of approximately factor 2. After averaging 7 frames per range (Figure 12), the range error is degraded from 3-4 cm for GSSS = 0.75 m to 5-13 cm for GSSS = 5.25 m (depending on SNR) which means an improvement compared the no averaging of nearly factor 3.

6. CONCLUSION

The following conclusions can be drawn from this analysis concerning the practical use of a GV system as a 3-D sensor. The gate length can be kept small because this reduces the number of required range steps in the sliding gates sequence to cover an entire target and a longer gate length does not enhance the range accuracy. Due to the strong impact of the SNR on the range error, enough energy per laser pulse should be sent to the target in order to achieve a sufficient SNR. Averaging several frames per range, significantly decreases the range error by a factor of 2-3.

If image acquisition is time limited, for example in dynamic scenarios, frame averaging is not useful for improving range accuracy. For instance, a gate length of 13.5 m without frame averaging (left graph in Figure 10) and a GSSS of 0.75 m result in a total number of images (and laser pulses) of 35 (35 ranges) and a range accuracy of 5-10 cm. A gate length of 13.5 m with averaging 4 frames per range (left graph in Figure 11) and a GSSS of 3 m result in a total number of images (and laser pulses) of 36 (9 ranges) and a range accuracy of 5-10 cm. A gate length of 13.5 m with averaging 7 frames per range (left graph in Figure 12) and a GSSS of 5.25 m result also in a total number of images (and laser pulses) of 35 (5 ranges) and a range accuracy of 5-13 cm. So, by limiting the acquisition time (and with a fixed laser pulse repetition rate also the total number of acquired frames) there is no improvement in range accuracy by frame averaging if the total number of images is constant.

If the image acquisition time is not limited, range accuracies below 5 cm are possible, for example for 4 averaged frames per range, 13.5 m gate length and GSSS = 0.75 m (left graph in Figure 11) or for 7 averaged frames per range, regardless of gate length and GSSS = 0.75 m (Figure 12).

REFERENCES

[1] Laurenzis, M., Christnacher, F., Monnin, D. and Scholz, T., "Investigation of range-gated imaging in scattering environments," Opt. Eng. 51(6), 061303, 1-6 (2012).

[2] Göhler, B. and Lutzmann, P., "Range accuracy of a Gated-Viewing system compared to a 3-D Flash LADAR under different turbulence conditions," Proc. SPIE 7835, 783504, 1-12 (2010)

[3] Repasi, E., Lutzmann, P., Steinvall, O., Elmqvist, M., Göhler, B. and Anstett, G., "Advanced short-wavelength infrared range-gated imaging for ground applications in monostatic and bistatic configurations," Appl. Opt. 48(31), 5956-5969 (2009).

[4] Andersson, P., "Long-range three-dimensional imaging using range-gated laser radar images," Opt. Eng. 45(3), 034301, 1-10 (2006).

[5] Busck, J., "Underwater 3-D optical imaging with a gated viewing laser radar," Opt. Eng. 44(11), 116001, 1-7 (2005).

[6] Laurenzis, M., Bacher, E., Metzger, N., Schertzer, S. and Christnacher, F., "Coding of range-gates with ambiguous sequences for extended three-dimensional imaging" Proc. SPIE 8542, 854204, 1-7 (2012)

[7] Laurenzis, M. and Bacher, E., "Image coding for three-dimensional range-gated imaging," Appl. Opt. 50(21), 3824-3828 (2011).

[8] Göhler, B. and Lutzmann, P., "Range accuracy of a Gated-Viewing system as a function of the number of averaged images" Proc. SPIE 8542, 854205, 1-8 (2012)

[9] Laurenzis, M., Lutz, Y., Christnacher, F., Matwyschuk, A. and Poyet, J.-M., "Homogeneous and speckle-free laser illumination for range-gated imaging and active polarimetry," Opt. Eng. 51(6), 061302, 1-8 (2012).

[10] Fried, D. L., "Time-delay-induced mean-square error in adaptive optics," J. Opt. Soc. Am. A 7(7), 1224-1225 (1990).